

# SCIENTIFIC REPORTS



OPEN

## Enhanced thermoelectric performance of $\beta$ -Zn<sub>4</sub>Sb<sub>3</sub> based nanocomposites through combined effects of density of states resonance and carrier energy filtering

Received: 24 July 2015  
Accepted: 06 November 2015  
Published: 15 December 2015

Tianhua Zou<sup>1,2</sup>, Xiaoying Qin<sup>1</sup>, Yongsheng Zhang<sup>1,3</sup>, Xiaoguang Li<sup>4,5</sup>, Zhi Zeng<sup>1,3</sup>, Di Li<sup>1</sup>, Jian Zhang<sup>1</sup>, Hongxing Xin<sup>1</sup>, Wenjie Xie<sup>2</sup> & Anke Weidenkaff<sup>2</sup>

It is a major challenge to elevate the thermoelectric figure of merit ZT of materials through enhancing their power factor (PF) and reducing the thermal conductivity at the same time. Experience has shown that engineering of the electronic density of states (eDOS) and the energy filtering mechanism (EFM) are two different effective approaches to improve the PF. However, the successful combination of these two methods is elusive. Here we show that the PF of  $\beta$ -Zn<sub>4</sub>Sb<sub>3</sub> can greatly benefit from both effects. Simultaneous resonant distortion in eDOS via Pb-doping and energy filtering via introduction of interface potentials result in a ~40% increase of PF and an approximately twofold reduction of the lattice thermal conductivity due to interface scattering. Accordingly, the ZT of  $\beta$ -Pb<sub>0.02</sub>Zn<sub>3.98</sub>Sb<sub>3</sub> with 3 vol.% of Cu<sub>3</sub>SbSe<sub>4</sub> nano-inclusions reaches a value of 1.4 at 648 K. The combination of eDOS engineering and EFM would potentially facilitate the development of high-performance thermoelectric materials.

Thermoelectric materials play an important role in cooling of electric devices and power generation from waste heat<sup>1–7</sup>. The conversion efficiency of a thermoelectric material is characterized by the figure of merit, ZT, defined as:  $ZT = (S^2/\rho\kappa)T$ , where S,  $\rho$ ,  $\kappa$  are the thermopower, electrical resistivity, and thermal conductivity, respectively. Typically, there are two ways to improve the ZT of thermoelectric materials: one is to lower the thermal conductivity  $\kappa$ <sup>8–12</sup> and the other is to boost the power factor  $PF = S^2/\rho$ <sup>13–16</sup>. While a variety of techniques is available to reduce the thermal conductivity, such as embedding nano-structures in bulk materials<sup>10,11</sup>, the fundamental challenge is to boost PF, for instance by increasing the thermopower S. According to the Mott equation, the thermopower S of a degenerate semiconductor can be expressed as:

<sup>1</sup>Key laboratory of Materials Physics, Institute of Solid State Physics, Chinese Academy of Sciences, 230031 Hefei, PR–China. <sup>2</sup>Institute of Materials Science, University of Stuttgart, 70569 Stuttgart, Germany. <sup>3</sup>University of Science and Technology of China, 230026 Hefei, PR–China. <sup>4</sup>Hefei National Laboratory for Physical Sciences at Microscale, Department of Physics, University of Science and Technology of China, Hefei 230026, P.R. China. <sup>5</sup>Collaborative Innovation Center of Advanced Microstructures, Nanjing University, Nanjing 210093, PR–China. Correspondence and requests for materials should be addressed to X.Q. (email: xyqin@issp.ac.cn) or Y.Z. (email: yshzhang@theory.issp.ac.cn)

$$\begin{aligned}
 S &= \frac{\pi^2 k_B^2 T}{3q} \left[ \frac{\partial \ln(\sigma(E))}{\partial E} \right]_{E=E_f} \\
 &= \frac{\pi^2 k_B^2 T}{3q} \left[ \frac{1}{p} \frac{\partial p(E)}{\partial E} + \frac{1}{\mu} \frac{\partial \mu(E)}{\partial E} \right]_{E=E_f}
 \end{aligned} \tag{1}$$

with the carrier mobility  $\mu(E) = q\tau/m_d^*$ , where  $\sigma$  is the electrical conductivity,  $q$  the carrier charge,  $E$  the energy,  $p(E)$  and  $\mu(E)$  energy dependent carrier density and mobility,  $\lambda$  the scattering parameter,  $k_B$  the Boltzmann constant,  $m_d^*$  the effective mass and  $E_f$  the Fermi energy. With the approximation of a free-electron gas and assuming an exponential dependence of the scattering parameter  $\lambda$  on the relaxation time  $\tau$ , i.e.  $\tau = \tau_0 E^{\lambda-1/2}$  (here  $\tau_0$  is an energy-independent constant), Eq.(1) can be written as:

$$S \approx \frac{\pi^2 k_B^2 T}{3q} \left[ \frac{N(E)}{p} + \frac{\lambda - \frac{1}{2}}{E} \right]_{E=E_f} \tag{2}$$

where  $N(E)$  is the electronic density of states (eDOS). Eq(2) implies that at a given carrier concentration,  $S$  can be enhanced by either increasing  $N(E)$ , i.e. the eDOS at the Fermi level, or the scattering parameter  $\lambda$ , which corresponds to the energy filtering mechanism (EFM)<sup>14</sup>. Heremans *et al.* showed that after Tl-doping of PbTe, its ZT is doubled due to the enhancement of the thermopower<sup>17</sup>. This is attributed to the resonant distortion of the eDOS. Accordingly, the recently observed enhanced thermopower of Pr and Sm doped  $\beta$ -Zn<sub>4</sub>Sb<sub>3</sub> can also be ascribed to the eDOS distortion of the host<sup>18,19</sup>.

On the other hand, Heremans *et al.* also observed an enhanced thermopower in PbTe-based nanocomposites containing Pb and Ag nanoparticles. This can be referred to the EFM<sup>20,21</sup> revealed by the increase of the scattering parameter  $\lambda$ . Only recently, Zou *et al.* experimentally proved that the introduction of Cu<sub>3</sub>SbSe<sub>4</sub> nanoinclusions increases the thermopower  $S$  of  $\beta$ -Zn<sub>4</sub>Sb<sub>3</sub> by EFM<sup>22</sup>. Theoretical studies indicate that the resulting interface potentials of semiconductor-based nanocomposites with semiconducting<sup>23</sup> or metallic<sup>24</sup> nanoinclusions stimulate the EFM. Although both resonant eDOS distortion and EFM have been used separately to enhance the thermopower  $S$  of a specific material, a successful application of both effects at the same time has not been reported so far.

In this study, we show that the two approaches can be combined to improve the thermoelectric performance of  $\beta$ -Zn<sub>4</sub>Sb<sub>3</sub>. As it is known,  $\beta$ -Zn<sub>4</sub>Sb<sub>3</sub> is one of the most promising thermoelectric materials on account of its low glasslike thermal conductivity and good electrical properties at moderate temperatures<sup>25-29</sup>; Cu<sub>3</sub>SbSe<sub>4</sub> is another important thermoelectric material with a narrow band gap<sup>9,30-32</sup>. In order to induce resonant distortion of the eDOS, we substituted Pb for Zn in  $\beta$ -Zn<sub>4</sub>Sb<sub>3</sub> forming  $\beta$ -(Zn<sub>1-x</sub>Pb<sub>x</sub>)<sub>4</sub>Sb<sub>3</sub> ( $x = 0, 0.01, 0.02, \text{ and } 0.03$ ). On the other hand, we synthesized  $\beta$ -(Zn<sub>1-x</sub>Pb<sub>x</sub>)<sub>4</sub>Sb<sub>3</sub>-based composites with Cu<sub>3</sub>SbSe<sub>4</sub> nanoinclusions to enhance energy filtering by creating interface potentials. Our results show that appropriate Pb-doping and Cu<sub>3</sub>SbSe<sub>4</sub> nanoinclusions both increase PF owing to an increased thermopower and significantly reduce (approx. 2-fold) the thermal conductivity of  $\beta$ -Zn<sub>4</sub>Sb<sub>3</sub>. This results in a large ZT of up to 1.4 at 648K of the nanocomposite  $f(\text{Cu}_3\text{SbSe}_4)/\beta\text{-Pb}_{0.02}\text{Zn}_{3.98}\text{Sb}_3$  with  $f = 3 \text{ vol.}\%$  (where  $f$  is the volumetric percentage of Cu<sub>3</sub>SbSe<sub>4</sub>).

## Results and Discussion

**Thermoelectric properties.** The temperature dependences of the electrical resistivity  $\rho$  of  $\beta$ -Zn<sub>4</sub>Sb<sub>3</sub>,  $\beta$ -(Zn<sub>1-x</sub>Pb<sub>x</sub>)<sub>4</sub>Sb<sub>3</sub> ( $x = 0.01, 0.02, \text{ and } 0.03$ ) and  $f(\text{Cu}_3\text{SbSe}_4)/\beta\text{-Pb}_{0.02}\text{Zn}_{3.98}\text{Sb}_3$  ( $f = 2, 3 \text{ and } 4 \text{ vol.}\%$ ) nanocomposite samples are shown in Fig. 1(a). The resistivity of each sample increases with temperature and reaches to a maximum at around 550 K. Further increasing temperature leads to a decrease of  $\rho$ . This reduction might be mainly ascribed to the onset of mixed conduction or thermal excitation of minority carriers<sup>18</sup>. Moreover, it can be noticed that the resistivities of both Pb-doped  $\beta$ -Zn<sub>4</sub>Sb<sub>3</sub> [ $\beta$ -(Zn<sub>1-x</sub>Pb<sub>x</sub>)<sub>4</sub>Sb<sub>3</sub> ( $x = 0, 0.01, 0.02, \text{ and } 0.03$ )] and the nanocomposite compounds [ $f(\text{Cu}_3\text{SbSe}_4)/\beta\text{-Pb}_{0.02}\text{Zn}_{3.98}\text{Sb}_3$  ( $f = 2, 3 \text{ and } 4 \text{ vol.}\%$ )] are much smaller compared to pristine  $\beta$ -Zn<sub>4</sub>Sb<sub>3</sub>.

The carrier concentrations determined by Hall coefficient measurements are given in Table 1. It can be seen that with  $x$  increasing from 0 to 0.01 and 0.02, the hole concentration of  $\beta$ -(Zn<sub>1-x</sub>Pb<sub>x</sub>)<sub>4</sub>Sb<sub>3</sub> increases from 12.1 to 13.6 and  $16.9 \times 10^{19} \text{ cm}^{-3}$ , respectively (see Table 1). With further increase of  $x$  to 0.03, the hole concentration slightly decreases to  $15.2 \times 10^{19} \text{ cm}^{-3}$ . As for the Cu<sub>3</sub>SbSe<sub>4</sub> containing composites [ $f(\text{Cu}_3\text{SbSe}_4)/\beta\text{-Pb}_{0.02}\text{Zn}_{3.98}\text{Sb}_3$  ( $f = 2, 3, 4 \text{ vol.}\%$ )] (Table 1), the carrier concentration varies from 18.4 to 22.4 and  $20.2 \times 10^{19} \text{ cm}^{-3}$  as the Cu<sub>3</sub>SbSe<sub>4</sub> content increases from 2 to 3 and 4 vol.%, respectively. In addition, the mobility  $\mu$  decreases moderately from 17.4 cm<sup>2</sup>/Vs to 15.1 cm<sup>2</sup>/Vs as  $f$  increases from 2 to 4 vol.%. These results indicate that the decrease of the resistivity with increasing inclusion content (see Fig.1 (a)) originates from the increased carrier concentration. Besides, the increase of the carrier concentration significantly exceeds the decrease of the mobility. The carrier concentration of  $f(\text{Cu}_3\text{SbSe}_4)/\beta\text{-Pb}_x\text{Zn}_{1-x}\text{Sb}_3$  for various values of  $x$  and  $f$  agrees with the resistivity trend in Fig.1 (a), indicating

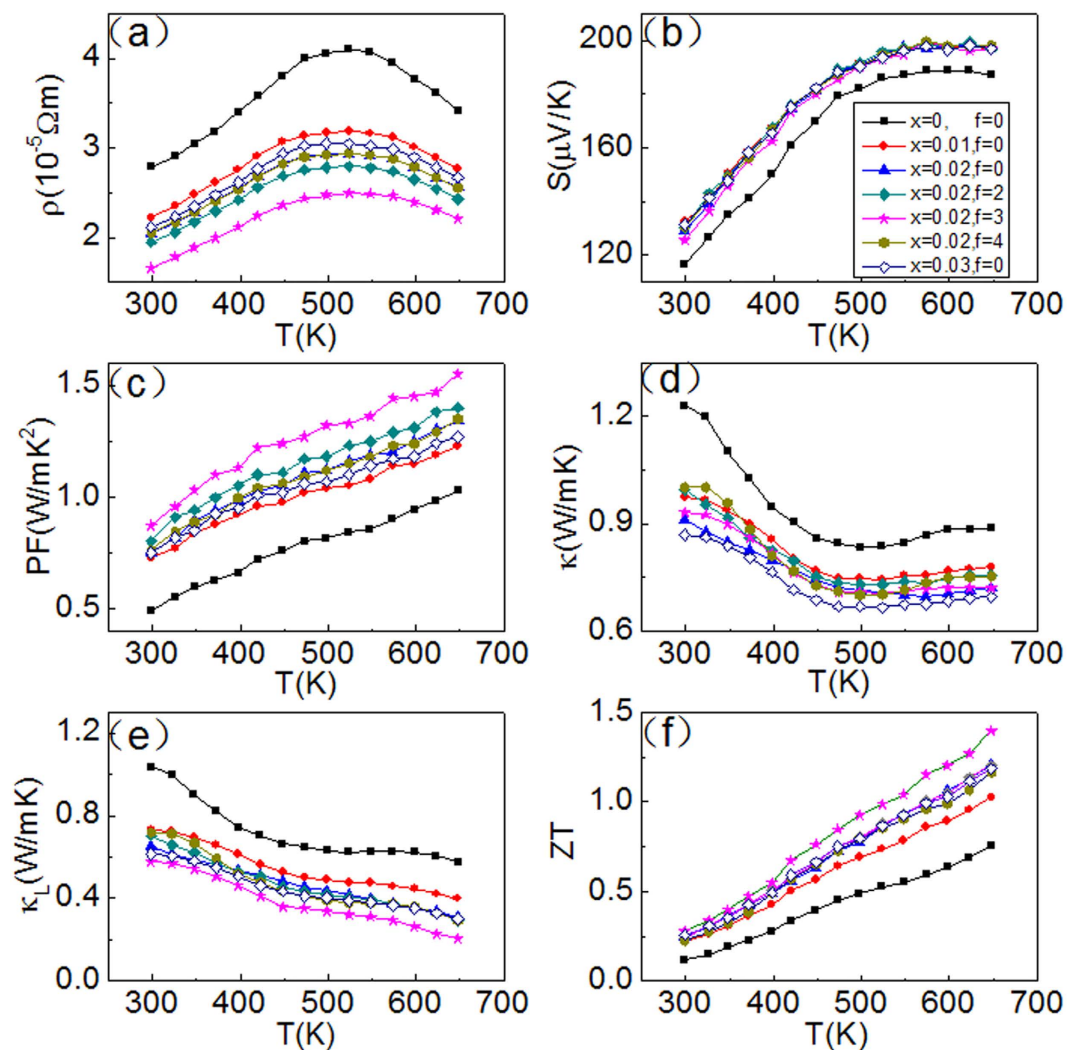


**Figure 1.** Temperature dependences of (a) electrical resistivity, (b) thermopower, (c) power factor, (d) total thermal conductivity, (e) lattice thermal conductivity, and (f) figure of merit ZT of  $\beta$ - $\text{Zn}_4\text{Sb}_3$ ,  $\beta$ - $(\text{Zn}_{1-x}\text{Pb}_x)_4\text{Sb}_3$  ( $x=0.01, 0.02$ , and  $0.03$ ) and  $f(\text{Cu}_3\text{SbSe}_4)/\beta$ - $\text{Pb}_{0.02}\text{Zn}_{3.98}\text{Sb}_3$  ( $f=2, 3$  and  $4$  vol.%) composite samples.

f(vol.%)	a(Å) <sup>a</sup>	c(Å) <sup>a</sup>	p( $10^{19}\text{cm}^{-3}$ ) <sup>b</sup>	$\mu(\text{cm}^2/\text{Vs})$ <sup>c</sup>	$m_d^*/m_e$ <sup>d</sup>	$\lambda$ <sup>e</sup>
x=0, f=0	12.207	12.420	12.1	18.6	1.51	0
x=0.01, f=0	12.220	12.423	13.6	20.7	1.91	0
x=0.02, f=0	12.224	12.431	16.9	18.1	2.14	0
x=0.03, f=0	12.227	12.420	15.2	19.4	2.04	0
x=0.02, f=2	12.220	12.423	18.4	17.4	2.14	0.18
x=0.02, f=3	12.220	12.423	22.4	16.8	2.14	0.30
x=0.02, f=4	12.220	12.423	20.2	15.1	2.14	0.28

**Table 1.** Physical parameters of  $\beta$ - $\text{Zn}_4\text{Sb}_3$ ,  $\beta$ - $(\text{Zn}_{1-x}\text{Pb}_x)_4\text{Sb}_3$  ( $x=0.01, 0.02$ , and  $0.03$ ) and  $f(\text{Cu}_3\text{SbSe}_4)/\beta$ - $\text{Pb}_{0.02}\text{Zn}_{3.98}\text{Sb}_3$  ( $f=2, 3$  and  $4$  vol.%) at room temperature (300K). <sup>a</sup>a and c are the lattice parameters. <sup>b</sup>p is the hole concentration. <sup>c</sup> $\mu$  is the Hall mobility. <sup>d</sup> $m_d^*/m_e$  is the ratio of the effective mass and the mass of the free electron. <sup>e</sup> $\lambda$  is the scattering parameter.

that the decrease of the resistivity with increasing doping and inclusion content originates from the changes of carrier concentration.

Figure 1(b) shows the temperature dependences of thermopower of  $\beta$ -Zn<sub>4</sub>Sb<sub>3</sub>,  $\beta$ -(Zn<sub>1-x</sub>Pb<sub>x</sub>)<sub>4</sub>Sb<sub>3</sub> ( $x = 0.01, 0.02, \text{ and } 0.03$ ) and  $f(\text{Cu}_3\text{SbSe}_4)/\beta$ -Pb<sub>0.02</sub>Zn<sub>3.98</sub>Sb<sub>3</sub> ( $f = 2, 3 \text{ and } 4 \text{ vol.}\%$ ) nanocomposite samples. Two points are particularly interesting: (1) Unlike the resistivity (Fig. 1(a)), the thermopower of all nanocomposite samples is nearly independent of the Pb and Cu<sub>3</sub>SbSe<sub>4</sub> content; (2) From the observed increased carrier concentration (Fig. 1(a)), a lower thermopower  $S$  of the Pb-doped samples and nanocomposite samples compared to pristine  $\beta$ -Zn<sub>4</sub>Sb<sub>3</sub> would be expected. Instead, we find that the thermopower of these samples obviously increases in the whole temperature range implying an increase of  $N(E)$  or/and  $\lambda$  (energy filtering effect) according to Eq. 2 (see below).

Because of the enhanced thermopower and decreased resistivity, all  $\beta$ -(Zn<sub>1-x</sub>Pb<sub>x</sub>)<sub>4</sub>Sb<sub>3</sub> ( $x = 0.01, 0.02, \text{ and } 0.03$ ) and  $f(\text{Cu}_3\text{SbSe}_4)/\beta$ -Pb<sub>0.02</sub>Zn<sub>3.98</sub>Sb<sub>3</sub> ( $f = 2, 3 \text{ and } 4 \text{ vol.}\%$ ) samples have a higher power factor  $PF (=S^2/\rho)$  than  $\beta$ -Zn<sub>4</sub>Sb<sub>3</sub> in the whole temperature range (Fig. 1(c)).  $f(\text{Cu}_3\text{SbSe}_4)/\beta$ -Pb<sub>0.02</sub>Zn<sub>3.98</sub>Sb<sub>3</sub> with  $f = 3 \text{ vol.}\%$  shows the largest value with  $PF = 1.55 \text{ W/mK}^2$  at 650 K, which is around 51% higher than that of pristine  $\beta$ -Zn<sub>4</sub>Sb<sub>3</sub>.

**Enhanced  $S$  by the resonant distortion of eDOS in Pb-doped  $\beta$ -(Zn<sub>1-x</sub>Pb<sub>x</sub>)<sub>4</sub>Sb<sub>3</sub>.** From these results we assume that the anomalously enhanced thermopower [Fig. 1(b)] of the nanocomposite samples is due to resonant distortion of the eDOS and the EFM, respectively. Evidence of the resonant distortion of the eDOS will be provided by means of the Pb-doped samples. Based on the measured values of carrier concentration  $p$  and thermopower  $S$ , the effective mass  $m_d^*$  is calculated. In the single parabolic band model,  $m_d^*$  and  $S$  can be approximated by<sup>33,34</sup>:

$$m_d^* = \frac{h^2}{2k_B T} \left( \frac{p}{4\pi F_{1/2}(\xi_F)} \right)^{2/3} \quad (3)$$

$$S = \frac{k_B}{e} \left[ \frac{[(\lambda + 2)F_{\lambda+1}(\xi_F)]}{[(\lambda + 1)F_{\lambda}(\xi_F)]} - \xi_F \right] \quad (4)$$

with the Fermi integral of order  $i$

$$F_i(\xi_F) = \int_0^\infty \frac{x^i}{1 + e^{(x-\xi_F)}} dx \quad (5)$$

where  $h$  is the Planck constant,  $\xi_F$  is the reduced Fermi level  $F_f/(k_B T)$  and  $\lambda$  is the scattering parameter. As mentioned by Heremans *et al.*, the scattering parameter  $\lambda$  of doped systems without inclusions (or secondary phase) is dominated by the acoustic modes and can be zeroed<sup>17</sup>. Table 1 summarizes the resulting effective mass  $m_d^*/m_e$  (where  $m_e$  is the free electron mass). At 300 K,  $m_d^*$  of un-doped  $\beta$ -Zn<sub>4</sub>Sb<sub>3</sub> is around 1.51  $m_e$ . The  $m_d^*$  of Pb-doped  $\beta$ -(Zn<sub>1-x</sub>Pb<sub>x</sub>)<sub>4</sub>Sb<sub>3</sub> ( $x = 0.01, 0.02, \text{ and } 0.03$ ) reaches 1.91  $m_e$ , 2.14  $m_e$ , and 2.04  $m_e$ , respectively, which is 1.26, 1.42, and 1.35 times larger than that of the un-doped sample. The large effective mass indicates the strong resonant distortion of the eDOS around the Fermi level, since the eDOS is directly related to effective mass  $m_d^*$  (for instance,  $N(E) = \frac{4\pi(2m_d^*)^{3/2}E^{1/2}}{h^3}$  for a free-electron gas)<sup>35</sup>.

Using formulae (3) and (4) and  $m_d^* = 1.51 m_e$  for the un-doped  $\beta$ -Zn<sub>4</sub>Sb<sub>3</sub>, we can plot the dependence of  $S$  on carrier concentration at 300K (black solid line in Fig. 2). Without resonant distortion of the eDOS Pb-doping, the thermopower  $S$  would be the same irrespective of the Pb-content and result in the same line. However, we find that  $S$  of  $\beta$ -(Zn<sub>1-x</sub>Pb<sub>x</sub>)<sub>4</sub>Sb<sub>3</sub> with  $x = 0.01, 0.02, \text{ and } 0.03$  is ~23, 31 and 29  $\mu\text{V/K}$  higher than the values of the black line, respectively (at 300K in Fig. 1(b)), indicating strong eDOS resonant distortion effects.

The origin of the resonant eDOS distortion caused by Pb substitution is determined by first principle calculations of the energy bands of pristine  $\beta$ -Zn<sub>4</sub>Sb<sub>3</sub> and Pb-doped  $\beta$ -Zn<sub>4</sub>Sb<sub>3</sub> (Fig. 3). The calculated result indicates that Pb-doping induces a strong sharp resonant peak near the Fermi level, which is mainly dominated by the Pb  $s$  orbitals (bottom of Fig. 3). The Pb  $p$  orbitals contribute little to the peak, which is due to the transfer of the outmost  $p$  electrons from Pb to Sb. The sharp peak indicates a larger effective mass ( $m_d^*$ ) and thermopower ( $S$ ) of the Pb-doped system compared to pristine  $\beta$ -Zn<sub>4</sub>Sb<sub>3</sub>.

Furthermore, the resonant distortion of the eDOS of  $\beta$ -(Zn<sub>1-x</sub>Pb<sub>x</sub>)<sub>4</sub>Sb<sub>3</sub> can also be quantified using the low-temperature heat capacity  $C_p$  of the samples. However, there are two temperature-dependent Zn<sub>4</sub>Sb<sub>3</sub> modifications, i.e.  $\beta$ -Zn<sub>4</sub>Sb<sub>3</sub> ( $T > 260 \text{ K}$ ) and  $\alpha$ -Zn<sub>4</sub>Sb<sub>3</sub> ( $T < 260 \text{ K}$ ), meaning that below ~260 K the  $\beta$  phase will transform to the  $\alpha$ -phase. As a result, one can only measure low-temperature heat capacity  $C_p$  of  $\alpha$ -Zn<sub>4</sub>Sb<sub>3</sub>. Nevertheless, previous work<sup>36</sup> showed that the eDOS patterns of the two Zn<sub>4</sub>Sb<sub>3</sub> modifications ( $\beta$  and  $\alpha$ ) are similar. Thus, it is appropriate to deduce the heat capacity (eDOS) of  $\beta$ -Zn<sub>4</sub>Sb<sub>3</sub> from the  $\alpha$ -Zn<sub>4</sub>Sb<sub>3</sub> measurements. The temperature dependence of the low temperature (<4K) heat capacity

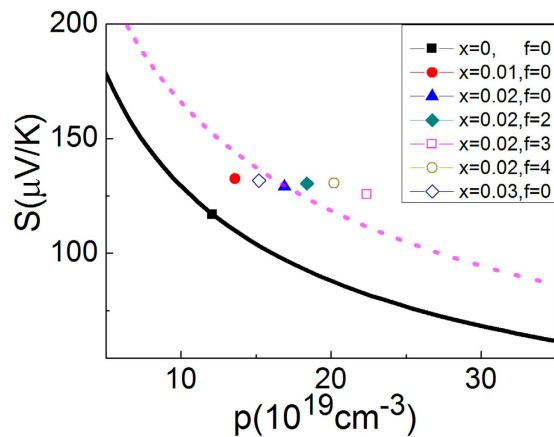


**Figure 2.** Variation of thermopower with carrier concentration of  $\beta$ -( $\text{Zn}_{1-x}\text{Pb}_x$ ) $_4\text{Sb}_3$  (0.01, 0.02, and 0.03) and  $f(\text{Cu}_3\text{SbSe}_4)/\beta\text{-Pb}_{0.02}\text{Zn}_{3.98}\text{Sb}_3$  ( $f = 2, 3$  and 4 vol.%) at 300K. The black solid and pink dashed lines represent the carrier concentration dependence of thermopower (Pisarenko relation) of  $\beta\text{-Zn}_4\text{Sb}_3$  using  $m_d^* = 1.51m_e$  and  $\beta\text{-Pb}_{0.02}\text{Zn}_{3.98}\text{Sb}_3$  using  $\lambda = 0$ , respectively.

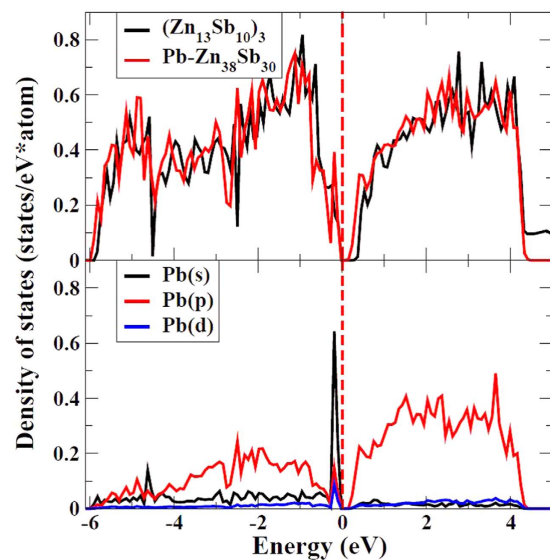


**Figure 3.** Top: Total electronic density of states (eDOS) of  $\beta\text{-Zn}_4\text{Sb}_3$  (or  $\text{Zn}_{13}\text{Sb}_{10}$ ) (black curve) and Pb-doped  $\beta\text{-Zn}_4\text{Sb}_3$  (red curve). Bottom: The itemized electronic density of states (pDOS) of Pb of Pb-doped  $\beta\text{-Zn}_4\text{Sb}_3$  compounds. The black, red and blue curves correspond to the pDOS of  $s$ ,  $p$  and  $d$  states, respectively. The sharp peak around the Fermi level is dominated by the Pb  $s$  state.

$C_p$  of a solid is expressed by  $C_p = \gamma T + bT^3$ , where the term  $bT^3$  stands for the lattice contribution and  $\gamma T$  for the charge carrier contribution with  $\gamma$  being related to  $N(E_f)$  (eDOS at the Fermi level)<sup>37</sup>:

$$\gamma = \frac{\pi^2}{3} k_B^2 N(E_f). \quad (6)$$

Hence, the slope of a  $C_p/T^3$  vs.  $1/T^2$  plot gives  $\gamma$ , which is directly proportional to the eDOS at the Fermi level. Figure 4 shows the  $C_p/T^3$  vs.  $1/T^2$  plots of un-doped  $\text{Zn}_4\text{Sb}_3$  ( $\alpha$  phase) and a typical doped compound  $(\text{Zn}_{1-x}\text{Pb}_x)_4\text{Sb}_3$  ( $x = 0.02$ ) ( $\alpha$  phase). The slope ( $\gamma$ ) of the plot of doped  $(\text{Zn}_{1-x}\text{Pb}_x)_4\text{Sb}_3$  is substantially larger than that of un-doped  $\text{Zn}_4\text{Sb}_3$ . Linear fitting in the low temperature regime yields the ratio  $\gamma_{\text{dop}}/\gamma_{\text{un-dop}} = N(E_f)_{\text{dop}}/N(E_f)_{\text{un-dop}} \sim 3.5$  (see Fig. 4) revealing that Pb-doping indeed significantly increases the eDOS at Fermi level. This is in agreement with the first principle calculation result shown in Fig. 3.

**Energy filtering effect induced by  $\text{Cu}_3\text{SbSe}_4$  nano inclusions in  $f(\text{Cu}_3\text{SbSe}_4)/\beta\text{-Pb}_{0.02}\text{Zn}_{3.98}\text{Sb}_3$ .** We calculated the scattering parameters  $\lambda$  (Table 1) of the nanocomposites using the effective mass



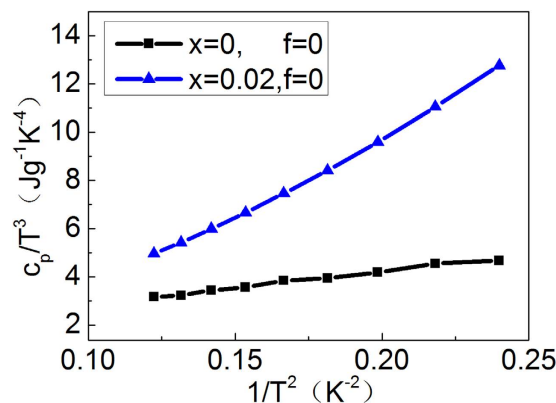


**Figure 4.**  $C_p/T^3$  vs  $1/T^2$  plots of  $Zn_4Sb_3$  ( $\alpha$  phase) and  $Pb_{0.02}Zn_{3.98}Sb_3$  ( $\alpha$  phase).

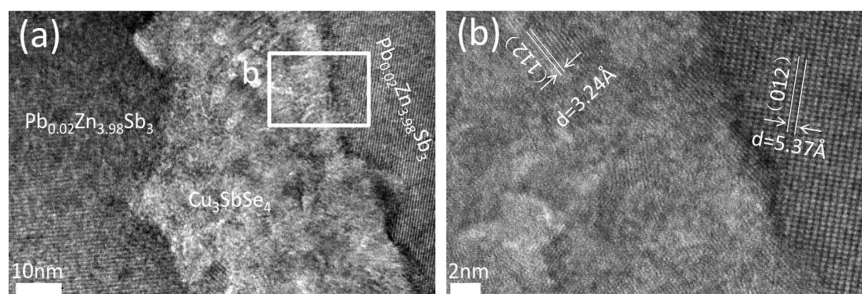


**Figure 5.** (a) Low-magnification bright-field image of  $f(Cu_3SbSe_4)/\beta-Pb_{0.02}Zn_{3.98}Sb_3$  with  $f = 3$  vol.%. (b) lattice image of the rectangle area in (a) showing the  $\beta-Zn_4Sb_3$  matrix (right),  $Cu_3SbSe_4$  inclusions (left) and a typical phase boundary (between the matrix and the dispersed phase).

$m_d^* = 2.14 m_e$  and the measured thermopower  $S$  values. The results are comparable to the those obtained by Heremans *et al.* with Ag/PbTe nanocomposites<sup>20</sup>. Scattering parameters of the composite samples are throughout larger than that of  $\beta-Pb_{0.02}Zn_{3.98}Sb_3$  (see Table 1) suggesting a higher thermopower of the nanocomposite samples. The carrier concentration dependence of the thermopower  $S$  of  $\beta-Pb_{0.02}Zn_{3.98}Sb_3$  ( $\lambda = 0$ ) at 300 K can be evaluated using formulae (3) and (4) yielding the pink dashed line in Fig. 2 (Pisarenko plot). Without energy filtering effect thermopower values of nanocomposites should lie on this pink line. Interestingly, the thermopower values of the  $f(Cu_3SbSe_4)/\beta-Pb_{0.02}Zn_{3.98}Sb_3$  ( $f = 2, 3$  and 4 vol.%) nanocomposites at 300 K are above the line ( $\sim 10, 15$  and  $12 \mu V/K$ , respectively) proving the enhanced energy filtering effect.

The above results indicate that the incorporation of nanophase  $Cu_3SbSe_4$  in the Pb-doped  $\beta-Zn_4Sb_3$  contributes to the large enhancement of  $S$  through the EFM. Microstructure analysis using high-resolution transmission electron microscopy (HRTEM) reveals the underlying mechanism. As shown in Fig.5(b), the Pb-doped  $\beta-Zn_4Sb_3$  matrix and the dispersed  $Cu_3SbSe_4$  particles are incoherently jointed at the phase boundary. Moreover, at room temperature the band gaps  $E_g$  of  $Cu_3SbSe_4$  and Pb-doped  $\beta-Zn_4Sb_3$  are  $0.3\text{--}0.4\text{ eV}$ <sup>31,38</sup> and  $0.26\text{ eV}$ <sup>39</sup>, respectively, leading to a valence band offset and the formation of p-p-type heterojunction barriers at the phase boundary. It is reasonable to assume that these potential barriers act as scattering centers giving rise to the EFM<sup>23</sup>. Hence, the enhanced thermopower of  $f(Cu_3SbSe_4)/\beta-Pb_{0.02}Zn_{3.98}Sb_3$  results from the two effects: the resonant distortion of the eDOS in the Pb-doped  $\beta-Pb_{0.02}Zn_{3.98}Sb_3$  matrix and the energy filtering effect at the phase boundaries confirming that it is feasible to combine both effects in one system.

The temperature dependence of  $\kappa$  of  $\beta-Zn_4Sb_3$ ,  $\beta-(Zn_{1-x}Pb_x)_4Sb_3$  ( $x = 0.01, 0.02$ , and  $0.03$ ) and  $f(Cu_3SbSe_4)/\beta-Pb_{0.02}Zn_{3.98}Sb_3$  ( $f = 2, 3$  and 4 vol.%) nanocomposite samples is shown in Fig.1(d). It can be seen that in the range of 300K to 500–550K,  $\kappa$  decreases with increasing temperature and then gradually increases as the temperature is further increased.  $\kappa$  includes the lattice thermal conductivity  $\kappa_L$  and the carrier contribution  $\kappa_c$ :  $\kappa = \kappa_L + \kappa_c$ . Thus,  $\kappa_L$  can be obtained by subtracting  $\kappa_c$  evaluated by the Wiedemann-Franz relation:  $\kappa_c = LT/\rho$ , where  $L$  is the Lorenz number. It is known that for heavily doped semiconductors,  $L$  is far below the Sommerfeld value  $L_0 = 2.45 \times 10^{-8} \Omega WK^{-2}$ , but depends on the reduced chemical potential  $\xi_B$ , the band structure and the scattering process. In the single parabolic band model the Lorenz number is expressed as<sup>33</sup>:

$$L = \frac{k_B^2 (1 + \lambda)(3 + \lambda) F_\lambda(\xi_F) F_{2+\lambda}(\xi_F) - (2 + \lambda)^2 F_{1+\lambda}(\xi_F)^2}{e^2 (1 + \lambda)^2 F_\lambda(\xi_F)^2} \quad (7)$$

where  $\xi_F$  is obtained by fitting the measured S data using Eq.(4). The evaluated L(T) curve is plotted in Fig.S4 (Supplementary Information). Due to phonon scattering at both the doped sites and the boundaries,  $\kappa_L$  of all  $\beta$ -(Zn<sub>1-x</sub>Pb<sub>x</sub>)<sub>4</sub>Sb<sub>3</sub> (x = 0.01, 0.02, and 0.03) and f(Cu<sub>3</sub>SbSe<sub>4</sub>)/ $\beta$ -Pb<sub>0.02</sub>Zn<sub>3.98</sub>Sb<sub>3</sub> (f = 2, 3 and 4 vol.%) samples is lower than that of the pristine  $\beta$ -Zn<sub>4</sub>Sb<sub>3</sub> (Fig. 1(e)). For instance, at 300K  $\kappa_L$  of the doped composite sample f(Cu<sub>3</sub>SbSe<sub>4</sub>)/ $\beta$ -Pb<sub>0.02</sub>Zn<sub>3.98</sub>Sb<sub>3</sub> with f = 3 vol.% is only 0.58 W/Km, which is approx. 40% smaller than that of the  $\beta$ -Zn<sub>4</sub>Sb<sub>3</sub> matrix.

Because of the simultaneous increase of PF and decrease of  $\kappa$ , the ZT values of all composite samples are enhanced compared to  $\beta$ -Zn<sub>4</sub>Sb<sub>3</sub>, as it is shown in Fig. 1(f). Specifically, 3 vol.% (Cu<sub>3</sub>SbSe<sub>4</sub>)/ $\beta$ -Pb<sub>0.02</sub>Zn<sub>3.98</sub>Sb<sub>3</sub> reached ZT = 1.4 at 648 K, which is about twice as large as that of  $\beta$ -Zn<sub>4</sub>Sb<sub>3</sub> studied here. This is the largest ZT value ever reported for a  $\beta$ -Zn<sub>4</sub>Sb<sub>3</sub>-based systems at 648 K<sup>34,40–42</sup>.

## Conclusions

We have demonstrated the enhancement of the thermoelectric properties as a result of two simultaneous effects: drastic reduction of the thermal conductivity and significant improvement of power factor. A figure of merit ZT = 1.4 at 648K could be achieved with f(Cu<sub>3</sub>SbSe<sub>4</sub>)/ $\beta$ -Pb<sub>0.02</sub>Zn<sub>3.98</sub>Sb<sub>3</sub> with f = 3 vol.%, which is the largest ZT value ever reported in a  $\beta$ -Zn<sub>4</sub>Sb<sub>3</sub>-based systems at 648 K. The enhanced thermopower of  $\beta$ -Pb<sub>0.02</sub>Zn<sub>3.98</sub>Sb<sub>3</sub>-based composites with Cu<sub>3</sub>SbSe<sub>4</sub> nanoinclusions results from the combination of resonant distortion of the eDOS in the Pb-doped matrix and intensified energy filtering at the heterojunction potential barriers. These findings provide a comprehensive way to design high-performance thermoelectric materials.

## Methods

$\beta$ -(Zn<sub>1-x</sub>Pb<sub>x</sub>)<sub>4</sub>Sb<sub>3</sub> (x = 0, 0.01, 0.02, and 0.03) samples were prepared from elemental Zn (99.9999%, powder), Sb (99.999%, powder) and Pb (99.9%, powder) in stoichiometric proportions. The elements were sealed in quartz tubes under vacuum (~10<sup>-3</sup> Pa). The tubes were heated to 1023 K for 12 h and then quenched in cool water. The  $\beta$ -(Zn<sub>1-x</sub>Pb<sub>x</sub>)<sub>4</sub>Sb<sub>3</sub> (x = 0, 0.01, 0.02, and 0.03) ingots were ground to powders by an agate mortar. To obtain Cu<sub>3</sub>SbSe<sub>4</sub> powders, constituent elements CuCl (99%, powder), SbCl<sub>3</sub>(99%, powder) and Se(99%, powder) were put into a glass beaker containing ethylenediamine. Then the collected powder was filtered, washed and dried in a vacuum oven. The nanometer-sized Cu<sub>3</sub>SbSe<sub>4</sub> and  $\beta$ -(Zn<sub>1-x</sub>Pb<sub>x</sub>)<sub>4</sub>Sb<sub>3</sub> (x = 0, 0.01, 0.02, and 0.03) powders were mixed for 4 h in a volume ratio of 2:98, 3:97, 4:96 in a planetary mill. The disk-shaped bulk nanocomposites were obtained by hot-pressing the blended powders at 600MPa in vacuum at 650 K for 1 h.

X-ray diffraction (Philips-X PERT PRO) with Cu K $\alpha$  radiation was used to check the phase constitutions. Scanning electron microscopy (SEM)(Hitachi S4800) equipped with an energy dispersive X-ray spectroscope (EDS) was used to analyze the microstructures of the composite samples. Moreover, microstructure investigations were also carried out using high-resolution transmission electron microscopy (HRTEM; JEOL JEM-2010) operating at a 200 kV accelerating voltage. Hall coefficients were measured by using a physical property measurement system (PPMS, Quantum Design). Low temperature heat capacity measurements were performed on the same instrument in the range of 2 K to 4 K. Electrical resistivity and thermopower were measured simultaneously by the standard four-probe method (ULVAC-RIKO: ZEM-3) in helium atmosphere from 300 K to 650 K. The thermal diffusivity  $\alpha$  was measured with a NETZSCH LFA-457 instrument in the temperature range of 300 K to 650 K. The thermal conductivity  $\kappa$  was calculated according to  $\kappa = DC_p\alpha$ , where  $C_p$  is the specific thermal capacity obtained by differential scanning calorimetry (DSC, perkin-Elmer) and D is the sample density measured by the Archimedes method.

DFT calculations were performed using the Vienna Ab Initio Simulation Package (VASP) with the projector augmented wave (PAW) scheme and the generalized gradient approximation of Perdew, Burke and Ernzerhof (GGA-PBE) for the electronic exchange-correlation functional. The energy cutoff for the plane wave expansion was 450 eV. The Brillouin zones were sampled by Monkhorst-Pack k-point meshes (3 × 3 × 2). Atomic positions and unit cell vectors were relaxed until all forces and components of the stress tensor were below 0.01 eV/Å and 0.2 kbar, respectively.

## References

1. Kraemer, D. *et al.* High-performance flat-panel solar thermoelectric generators with high thermal concentration. *Nat. Mater.* **10**, 532–538 (2011).
2. Chen, C., Yang, B. & Liu, W. Engineering nanostructures for energy conversion. *Heat Transfer and Fluid Flow in Microscale and Nanoscale Structures*, (eds Faghri, M. & Sundén, B.) Ch. 5, 45–92 (UK: WIT Press, Southampton, 2004).
3. Yang, B., Ahuja, H. & Tran, T. N. Review Article: Thermoelectric Technology Assessment: Application to Air Conditioning and Refrigeration. *HVAC&R Res.* **14**, 635–653 (2008).
4. Snyder, G. J. & Toberer, E. S. Complex thermoelectric materials. *Nat. Mater.* **7**, 105–114 (2008).
5. Wang, S. *et al.* Conductivity-limiting bipolar thermal conductivity in semiconductors. *Sci. Rep.* **5**, 10136 (2015).
6. Pei, Y. *et al.* Convergence of electronic bands for high performance bulk thermoelectrics. *Nature* **473**, 66–69 (2011).

7. Zhao, L. D. *et al.* Ultralow thermal conductivity and high thermoelectric figure of merit in SnSe crystals. *Nature* **508**, 373–377 (2014).
8. Zhang, Y. *et al.* First-principles description of anomalously low lattice thermal conductivity in thermoelectric Cu-Sb-Se ternary semiconductors. *Phys. Rev. B* **85**, 054306 (2012).
9. Zhang, Y., Ozoliņš, V., Morelli, D. & Wolverton, C. Prediction of New Stable Compounds and Promising Thermoelectrics in the Cu-Sb-Se System. *Chem. Mater.* **26**, 3427–3435 (2014).
10. Hsu, K. F. *et al.* Cubic  $\text{AgPb}_m\text{SbTe}_{2+m}$ : bulk thermoelectric materials with high figure of merit. *Science* **303**, 818–821 (2004).
11. Kanatzidis, M. G. Nanostructured Thermoelectrics: The New Paradigm?†. *Chem. Mater.* **22**, 648–659 (2010).
12. Kim, W. *et al.* Thermal Conductivity Reduction and Thermoelectric Figure of Merit Increase by Embedding Nanoparticles in Crystalline Semiconductors. *Phys. Rev. Lett.* **96**, 04590 (2006).
13. He, J., Kanatzidis, M. G. & Dravid, V. P. High performance bulk thermoelectrics via a panoscopic approach. *Mater. Today* **16**, 166–176 (2013).
14. Minnich, A. J., Dresselhaus, M. S., Ren, Z. F. & Chen, G. Bulk nanostructured thermoelectric materials: current research and future prospects. *Energy Environ. Sci.* **2**, 466 (2009).
15. Lan, Y., Minnich, A. J., Chen, G. & Ren, Z. Enhancement of Thermoelectric Figure-of-Merit by a Bulk Nanostructuring Approach. *Adv. Funct. Mater.* **20**, 357–376 (2010).
16. Heremans, J. P., Wiedlocha, B. & Chamoire, A. M. Resonant levels in bulk thermoelectric semiconductors. *Energy Environ. Sci.* **5**, 5510 (2012).
17. Heremans, J. P. *et al.* Enhancement of thermoelectric efficiency in PbTe by distortion of the electronic density of states. *Science* **321**, 554–557 (2008).
18. Wang, Q. Q. *et al.* Resonant distortion of electronic density of states and enhancement of thermoelectric properties of  $\beta\text{-Zn}_4\text{Sb}_3$  by Pr doping. *J. Appl. Phys.* **113**, 124901 (2013).
19. Wang, Q. Q., Qin, X. Y., Li, D. & Zou, T. H. Enhancement of thermopower and thermoelectric performance through resonant distortion of electronic density of states of  $\beta\text{-Zn}_4\text{Sb}_3$  doped with Sm. *Appl. Phys. Lett.* **102**, 154101 (2013).
20. Heremans, J., Thrush, C. & Morelli, D. Thermopower enhancement in lead telluride nanostructures. *Phys. Rev. B* **70**, 115334 (2004).
21. Heremans, J. P., Thrush, C. M. & Morelli, D. T. Thermopower enhancement in PbTe with Pb precipitates. *J. Appl. Phys.* **98**, 063703 (2005).
22. Zou, T. H. *et al.* Simultaneous enhancement in thermoelectric power factor and phonon blocking in hierarchical nanostructured  $\beta\text{-Zn}_4\text{Sb}_3\text{-Cu}_3\text{SbSe}_4$ . *Appl. Phys. Lett.* **104**, 013904 (2014).
23. Yang, X. H. *et al.* Enhanced thermopower and energy filtering effect from synergetic scattering at heterojunction potentials in the thermoelectric composites with semiconducting nanoinclusions. *J. Alloy. Compd.* **558**, 203–211 (2013).
24. Liu, M. & Qin, X. Y. Enhanced thermoelectric performance through energy-filtering effects in nanocomposites dispersed with metallic particles. *Appl. Phys. Lett.* **101**, 132103 (2012).
25. Snyder, G. J., Christensen, M., Nishibori, E., Caillat, T. & Iversen, B. B. Disordered zinc in  $\text{Zn}_4\text{Sb}_3$  with phonon-glass and electron-crystal thermoelectric properties. *Nat. Mater.* **3**, 458–463 (2004).
26. Zhu, G. *et al.* The effect of secondary phase on thermoelectric properties of  $\text{Zn}_4\text{Sb}_3$  compound. *Nano Energy* **2**, 1172–1178 (2013).
27. Wang, S. *et al.* Enhanced Thermoelectric Performance and Thermal Stability in  $\beta\text{-Zn}_4\text{Sb}_3$  by Slight Pb-Doping. *J. Electron. Mater.* **41**, 1091–1099 (2012).
28. Li, D. & Qin, X. Effects of Te doping on the transport and thermoelectric properties of  $\text{Zn}_4\text{Sb}_3$ . *Intermetallics* **19**, 1651–1655 (2011).
29. Li, D., Hng, H., Ma, J. & Qin, X. Effects of Nb doping on thermoelectric properties of  $\text{Zn}_4\text{Sb}_3$  at high temperatures. *J. Mater. Res.* **24**, 430–435 (2009).
30. Li, D. *et al.* Co-precipitation synthesis of nanostructured  $\text{Cu}_3\text{SbSe}_4$  and its Sn-doped sample with high thermoelectric performance. *Dalton Trans.* **43**, 1888–1896 (2014).
31. Wei, T.-R. *et al.* Thermoelectric properties of Sn-doped p-type  $\text{Cu}_3\text{SbSe}_4$ : a compound with large effective mass and small band gap. *J. Mater. Chem. A* **2**, 13527 (2014).
32. Li, Y. *et al.* Transport properties and enhanced thermoelectric performance of aluminum doped  $\text{Cu}_3\text{SbSe}_4$ . *RSC Adv.* **5**, 31399–31403 (2015).
33. Xie, H. *et al.* Beneficial Contribution of Alloy Disorder to Electron and Phonon Transport in Half-Heusler Thermoelectric Materials. *Adv. Funct. Mater.* **23**, 5123–5130 (2013).
34. Caillat, T., Fleurial, J.-P. & Borshchevsky, A. Preparation and thermoelectric properties of semiconducting  $\text{Zn}_4\text{Sb}_3$ . *J. Phys. Chem. Solids* **58**, 1119–1125 (1997).
35. Kittel, C. *Introduction to solid state physics*. 8<sup>th</sup> edn, Ch. 6, 131–157 (New York: Wiley, 2005).
36. Nylén, J., Andersson, M., Lidin, S. & Häussermann, U. The structure of  $\alpha\text{-Zn}_4\text{Sb}_3$ : ordering of the phonon-glass thermoelectric material  $\beta\text{-Zn}_4\text{Sb}_3$ . *J. Am. Chem. Soc.* **126**, 16306–16307 (2004).
37. Liu, W. *et al.* Convergence of Conduction Bands as a Means of Enhancing Thermoelectric Performance of n-Type  $\text{Mg}_2\text{Si}_{1-x}\text{Sn}_x$  Solid Solutions. *Phys. Rev. Lett.* **108**, 166601 (2012).
38. Yang, C. Y., Huang, F. Q., Wu, L. M. & Xu, K. New stannite-like p-type thermoelectric material  $\text{Cu}_3\text{SbSe}_4$ . *J. Phys. D Appl. Phys.* **44**, 295404 (2011).
39. Qiu, A. N., Zhang, L. T. & Wu, J. S. Crystal structure, electronic structure, and thermoelectric properties of  $\beta\text{-Zn}_4\text{Sb}_3$  from first principles. *Phys. Rev. B* **81**, 035203 (2010).
40. Lin, J. P. *et al.* Unexpected High-Temperature Stability of beta- $\text{Zn}_4\text{Sb}_3$  Opens the Door to Enhanced Thermoelectric Performance. *J. Am. Chem. Soc.* **136**, 1497–1504 (2014).
41. Yin, H. *et al.* Highly enhanced thermal stability of  $\text{Zn}_4\text{Sb}_3$  nanocomposites. *Chem. Commun.* **49**, 6540–6542 (2013).
42. Cui, J., Fu, H., Mao, L., Chen, D. & Liu, X. Effects of  $\text{Cu}_3\text{Zn}_3$  addition on the thermoelectric properties of  $\text{Zn}_4\text{Sb}_3$ . *J. Appl. Phys.* **106**, 3702 (2009).

## Acknowledgements

The authors thank Prof. Dr. G. Schmitz (University of Stuttgart) for useful discussions. Financial support was provided by the National Natural Science Foundation of China (Nos. 11174292, 11374306, 51101150, 11474283 add 21521001), the Major/Innovative Program of the Development Foundation of Hefei Center for Physical Science and Technology No. 2014FXCX001, One Hundred Person Project of the Chinese Academy of Sciences No. Y54N251241, the National Basic Research Program of China (973 program) under Projects 2012CB922003 and 2015CB921201 and the Deutsche Forschungsgemeinschaft under the DFG Priority Program SPP 1386 (Grant WE 2803/2-2).



### Author Contributions

T.Z. wrote the main manuscript text. X.Q. designed the experiments and analyzed data. X.L. was responsible for measuring the low-temperature heat capacity. Y.Z and Z.Z. contributed to the first-principles calculation. D.L., J.Z., H.X., W.X. and A.W. revised the manuscript. All authors reviewed the manuscript.

### Additional Information

**Supplementary information** accompanies this paper at <http://www.nature.com/srep>

**Competing financial interests:** The authors declare no competing financial interests.

**How to cite this article:** Zou, T. *et al.* Enhanced thermoelectric performance of  $\beta$ -Zn<sub>4</sub>Sb<sub>3</sub> based nanocomposites through combined effects of density of states resonance and carrier energy filtering. *Sci. Rep.* 5, 17803; doi: 10.1038/srep17803 (2015).



This work is licensed under a Creative Commons Attribution 4.0 International License. The images or other third party material in this article are included in the article's Creative Commons license, unless indicated otherwise in the credit line; if the material is not included under the Creative Commons license, users will need to obtain permission from the license holder to reproduce the material. To view a copy of this license, visit <http://creativecommons.org/licenses/by/4.0/>